Determination of the Total Texture Function from Individual Orientation Measurements by Electron Backscattering Pattern

T Baudin, R Penelle

Determination of the Total Texture Function from Individual Orientation Measurements by Electron Backscattering Pattern

T. BAUDIN and R. PENELLE

The orientation distribution function (ODF) calculation is usually performed using pole figures measured by X-ray or neutron diffraction. However, this kind of experimental technique does not allow total ODF to be determined, since the odd terms of the series expansion are not directly accessible from pole figures. The individual orientation measurement technique can be used, but it is necessary to evaluate the right orientation number necessary for a statistically reliable ODF. For samples at the surface, at the fifth of thickness from the surface and at the center of a Fe 3 pct Si sheet, this study shows that only 100 orientations are sufficient to find the principal components of the texture, but this number must be increased by a factor of 10 to evaluate with rather good accuracy the heights of the peaks. Indeed, to obtain a good correlation with an ODF calculated from pole figures measured by X-ray diffraction, the number of orientations needed is about 1000.

I. INTRODUCTION

FOR some years, researchers have been very interested in the characterization of (local and global) texture from individual orientation measurements. The actual studies have the following two aims.

(1) The first one consists of "local relative studies" which allow one to show the crystallographic orientation of one or several grains in a polycrystal and then the misorientation between these grains. These studies lead also to very interesting crystallographic and microstructural results, such as the orientation of grains near a failure, the evolution of the orientation of single crystal during deformation, *etc.*

(2) The second one, which consists of a "global absolute study," allows one to establish statistical functions (orientation distribution function (ODF), misorientation function, position function, correlation function, *etc.*). For this, it is necessary to measure both the crystallographic orientation and the shape and size (microstructure) of each grain and also to characterize some parameters, such as the shape of modeled orientations and the number of measurements to determine functions which are statistically admissible.

One of these functions is the ODF which cannot be totally calculated by global techniques, such as X-ray or neutron diffraction, since only the even part of the series expansion can be determined. A first solution consists of using the mathematical method which allows one to evaluate the odd part by using the even part of the ODF knowing that the total function is the sum of the even and odd parts. A second method consists of evaluating the parts of this function using individual orientations which are modeled by Gaussian functions. The aim of this study is to compare these different methods and, in particular, to try to determine the number of orientations necessary to calculate a total ODF.

II. DETERMINATION OF THE TEXTURE FUNCTION

A. *Calculation Principle*

The ODF is generally calculated using pole figures measured by X-ray or neutron diffraction techniques. The fundamental relation linking pole density to the ODF can be solved by different methods:

(1) the Bunge[1,2] or the Roe[3,4] method using the series expansion (harmonic method);
(2) the discretization method[5–8] (vector method);
(3) the probabilistic method;[9,10,11] and
(4) the integral transformation method[12] (inversion formula).

The first approach is used for this study and is described using the Roe formalism.

B. *Harmonic Method*

With the global (X-ray or neutron diffraction) or local electron backscattering pattern (EBSP) analysis, it is necessary to resolve the following equation:

$$F(g) = \sum_{l=0}^{\infty} \sum_{m=-l}^{l} \sum_{n=-l}^{l} f_{lmn} T_{mn}^{l}(g) \qquad [1]$$

where $F(g)$ is the ODF expressed in the Euler space, g is an orientation characterized by the ψ, θ, and φ angles (Roe notation), T_{mn}^{l} (g) is the generalized spherical harmonic function, and the f_{lmn} are the coefficients of the ODF which can be estimated from pole figures measured by X-ray or neutron diffraction or from individual orientation measurements.

1. *X-ray or neutron diffraction*

The fundamental relation which links the pole density to the ODF must be solved:

$$q(\eta,\chi) = \int_{0}^{2\pi} F(g)d\gamma \qquad [2]$$

where $q(\eta,\chi)$ is the pole density at a point defined by the η and χ spherical coordinates on the $\{hkl\}$ pole figure and $d\gamma$ is the differential element of a rotation around the normal of the diffracting plane.

These two functions, $q(\eta,\chi)$ and $F(g)$, can be expanded on the spherical harmonics basis. After expanding the integral defined in Eq. [2], a relation is obtained between the pole density and the f_{lmn} coefficients; thus,

$$q(\eta,\chi) = \sum_{l}\sum_{m}\sum_{n} 2\pi \left(\frac{2}{2l+1}\right)^{1/2} \cdot f_{lmn}\, Y_l^n{}^*(h_i)\, Y_l^m(\eta,\chi) \qquad [3]$$

where $Y_l^n(h_i)$ and $Y_l^m(\eta,\chi)$ are surface spherical harmonics (the asterisk denotes the complex conjugate) and h_i corresponds to the $\{hkl\}$ Miller indices of the ith pole figure.

However, this kind of diffraction technique does not allow the separation of $+h_i$ and $-h_i$ directions of centrosymmetric crystals, and so, in fact, the measured pole figure is the superposition of two parts corresponding, respectively, to the pole figure of the equivalent direction $+h$ and $-h$; therefore,

$$\bar{q}(\eta,\chi) = \frac{1}{2}\left[q_{+h}(\eta,\chi) + q_{-h}(\eta,\chi)\right] \qquad [4]$$

with

$$q_{+h}(\eta,\chi) = q_{-h}(\eta,\chi)$$

Then, Eq. [3] can be expressed as

$$\bar{q}(\eta,\chi) = \sum_{l}\sum_{m}\sum_{n} 2\pi \left(\frac{2}{2l+1}\right)^{1/2} \cdot \bar{f}_{lmn}\, Y_l^n{}^*(h_i)\, Y_l^m(\eta,\chi) \qquad [5]$$

Bunge[2] has shown that the $\bar{f}_{lmn}$ coefficients (or $\bar{C}_l^{\mu\nu}$ using his notation) which describe a virtual texture can be written as

$$\bar{C}_l^{\mu\nu} = C_l^{\mu\nu}\,[1 + (-1)^l]/2 \quad \begin{cases} = C_l^{\mu\nu} \text{ for } l \text{ even} \\ = 0 \text{ for } l \text{ odd} \end{cases}$$

This last relation shows that the odd part of the ODF cannot be directly determined using pole figures. Moreover, this indeterminacy can lead to the appearance of ghost components which lack physical meaning due to the absence of the odd part of the total ODF.

2. *Single orientation measurement*

The f_{lmn} (Eq. [1]) can be calculated from individual orientation measurements. The first problem is determining how to model each orientation.

Bunge[1,2] proposed to model each orientation g_i with a Dirac function, the total function $F(g)$ being the sum of N Dirac functions. However, Wagner[13] showed that this approach leads to negative domains (linked to truncation effects, since the series expansion is calculated for a finite L value), knowing that, by definition, the total ODF, which is the sum of even $\bar{F}(g)$ and odd $\tilde{F}(g)$ functions, is always positive or equal to zero:

$$F(g) = \bar{F}(g) + \tilde{F}(g) \geq 0 \qquad [6]$$

Some authors have proposed[14–18] the use of Gaussian functions and to express the f_{lmn} coefficients as

$$f_{lmn} = \frac{1}{N} \sum_{i=1}^{N} K\, T^{l}_{mn}{}^{*}(g_i) \qquad [7]$$

with

$$K = \frac{\exp(-l^2\Phi_0^2/4) - \exp[-(l+1)^2\Phi_0^2/4]}{1 - \exp(-\Phi_0^2/4)} \qquad [8]$$

The Φ_0 parameter is linked to the width at the halfheight b of the Gaussian by the relation

$$\Phi_0 = b/2\sqrt{\ln 2} \qquad [9]$$

Moreover, Wagner[13] has shown that Φ_0 can be linked to a p parameter characterizing the texture sharpness and to the number (N) of measured individual orientations. So, for a cubic material and a triclinic texture, Wright and Adams[19] have found the relation

$$\Phi_0 = \left(\frac{\pi p}{2N}\right)^{1/3} \qquad [10]$$

The value of p must be equal to one for a random texture and tends toward zero for a strong texture. For intermediate textures, which is the case in the present study, p is taken equal to 0.5 (see, for example, Reference 13 in the case of rhombohedral materials and Reference 19 in the case of a cubic material). Consequently, the Φ_0 expression (Eq. [10]) allows one to determine the Gaussian shape in terms of the number of measured individual orientations.

It is now known that the influence of the odd ODF is not negligible relative to the even ODF (see, for example, Reference 12). For example, Figure 1 shows the sections at $\varphi = 0$ deg of $\bar{F}(g)$, $\bar{\bar{F}}(g)$, and $F(g)$ in the (ψ,θ) plane, calculated for the brass component {011}⟨211⟩, with $\Phi_0 = 6$ deg ($b = 10$ deg) and $L = 34$. Let us remark that the imposed orientation is obviously found again, but, moreover, other components without physical meaning appear in the section of $\bar{F}(g)$ (Figure 1(a)). However, the "mirror pictures" of these components appear in the section of $\bar{\bar{F}}(g)$ (Figure 1(b)) and therefore disappear in the section of $F(g)$. On this last section,

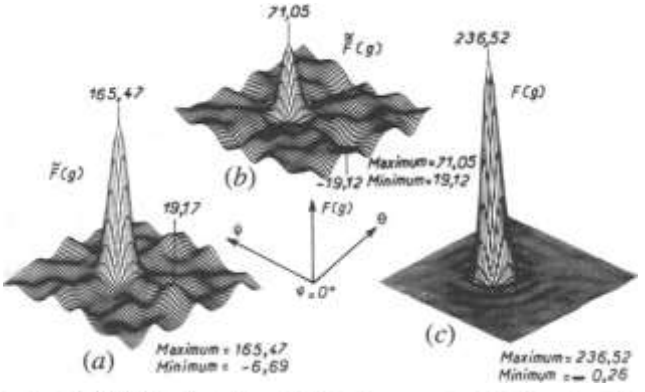

Fig. 1—{011}⟨211⟩ orientation—HM: (*a*) even part, (*b*) odd part, and (*c*) total texture function.

there remain imperfections, such as little positive or negative domains (in these domains, the absolute value of $F(g)$ is less than 0.5); these are only due to the truncation error.

C. *Mathematical Method*

The example described in Section B led some authors to propose mathematical methods (MMs) to evaluate the odd part of the ODF calculated from pole figures.

If $\bar{F}(g) < 0$, then $\bar{\bar{F}}(g) = -\bar{F}(g)$; *i.e.*, the positivity condition of $F(g)$ is verified. This condition must also suppress some positive peaks of $\bar{F}(g)$ which have no physical significance; so, for a given positive value of $\bar{F}(g)$, the same relation ($\bar{\bar{F}}(g) = -\bar{F}(g)$) has to be used. In these conditions, Dahms and Bunge[20] have proposed a method which is a refinement of the zero range method (see Esling[21]). One of the advantages of this method is that experimentally determined even terms are retained.

Let us note that other methods not used here have been proposed by Van Houtte[22] who developed the quadratic method and by Wang *et al.*[23] who developed the maximum entropy method.

The principle of this MM (see also Bunge[24]) consists of calculating the nth order approximation of $F(g)$, *i.e.*, ${}^{(n)}F(g)$, with the relation

$$ {}^{(n)}F(g) = {}^{(n-1)}F(g) + {}^{(n)}\bar{\bar{F}}(g) \qquad [11] $$

with

$$ {}^{(0)}F(g) = \bar{F}(g) \qquad [12] $$

where ${}^{(n)}\hat{F}(g)$ is defined according to

$$ {}^{(n)}\hat{F}(g) = \begin{cases} -{}^{(n-1)}F(g) & \text{for } {}^{(n-1)}F(g) < 0 \\ 0 & \text{for } {}^{(n-1)}F(g) \geq 0 \end{cases} \qquad [13] $$

and ${}^{(n)}$ denotes the odd part of ${}^{(n)}\hat{F}(g)$ and allows calculation of the $\bar{\bar{f}}_{lmn}$ coefficients:

$$ \bar{\bar{f}}_{lmn} = \int {}^{(n)}\bar{\bar{F}}(g) T^{l}_{mn}(g) dg \qquad [14] $$

and the ${}^{(n)}F(g)$ function necessary to continue the calculation (Eq. [11]). These authors have also generalized this method assuming that a condition $F(g) > r_{min}$ can be used, which means that a solution is sought with a given "background" ($0 < r_{min} < 1$). It is evident that this procedure can only converge if a solution with the properties defined by Eq. [15] really exists.

$$ {}^{(n)}\hat{F}(g) = \begin{cases} -{}^{(n-1)}F(g) + r_{min} & \text{for } {}^{(n-1)}F(g) < r_{min} \\ 0 & \text{for } {}^{(n-1)}F(g) \geq r_{min} \end{cases} \qquad [15] $$

Wagner *et al.*[25] have tried to analyze the effect of the r_{min} choice on the determination of the complete ODF and have shown that $r_{min} = q(\eta,\chi)_{min}$ knowing that $F(g)_{min} \leq q(\eta,\chi)_{min}$.

This result is a very interesting approximation of the true ODF in the case of a theoretical example which Wagner *et al.* presented (Table I). However, their method does not seem to modify the results of a real texture of

Table I. Evolution of $F(g)_{max}$ and $F(g)_{min}$ in Terms of r

	r	$F(g)_{max}$	$F(g)_{min}$
Theoretical total ODF	—	5.04	0.72
Calculation	0.00	4.00	0.10
Calculation	0.72	5.00	0.72

a low-carbon steel, since the variations of $F(g)_{max}$ and $F(g)_{min}$ are very slow in terms of r_{min}.

D. *S. Matthies Method*

The two previously described methods are based on the use of the harmonic method which leads to truncation error, since some series expansions are performed to a finite L value. To suppress this problem, the S. Matthies method (SMM) allows an exact solution to be determined.

For that, Matthies *et al.*[12] use the relation

$$F(S,\bar{\omega}) = N(S)e^{S\cos\bar{\omega}} \qquad [16]$$

with

$$\bar{\omega} = \bar{\omega}(g_0,g) \qquad \text{and} \qquad 0 \le S \le \infty$$

$F(S,\bar{\omega})$ represents the total texture function (or $F(g)$) calculated for a given orientation (g_0) modeled by a Gaussian function in the G (Euler) space ($g \in G$). The term $N(S)$ is a constant of normalization calculated using Bessel functions (see Matthies *et al.*[12]). The S parameter allows one to characterize the g_0 orientation shape. For $S = 0$, Eq. [16] describes a random distribution, and if S tends to infinity, the orientation is modeled by a Dirac function. The term S is linked to the b parameter by the relation

$$S = \ln 2/[2\sin^2(b/4)] \qquad [17]$$

with

$$b \le 2\pi$$

If $b \ll \pi$ ($S \gg 1$), Eq. [16] becomes the same as that proposed by Bunge,[2] a traditional Gauss distribution:

$$F(\Phi_0,\bar{\omega}) = N(\Phi_0)e^{-(\bar{\omega}/\Phi_0)^2} \qquad [18]$$

This approach also allows calculation of $\bar{F}(g)$ (and so $\tilde{F}(g)$) using $F(g)$ and a ghost function $F_G(g)$ expressed with Bessel functions:

$$\bar{F}(g) = \frac{F(g)}{2} + F_G(g) \qquad [19]$$

We note that it is possible to express $F_G(g)$ using the f_{lmn} coefficients (see Esling[21]) of the HM, but we find again the truncation problem.

To illustrate the interest in this kind of calculation, we use this method to determine, for the {011}⟨211⟩ orientation, first $F(g)$, then $\bar{F}(g)$, after having calculated $F_G(g)$, and finally $\tilde{F}(g)$, which are presented, respectively, in Figures 2(c), (b), and (a). It is interesting to see that the maximal values of these functions are higher than those determined with the harmonic method (HM), indicating that the series calculation with $L = 34$ is not sufficient.

Moreover, if $g(g \in G)$ is far from g_0, then the background is taken equal to zero and the waves observed on Figure 1(c) vanish on Figure 2(c).

E. *Discussion*

In the case of a single orientation, the truncation error is obviously very important when the HM is used; thus, it is more interesting to use the S.M.M. which gives an exact solution. However, for polycrystal materials, it becomes difficult to compare the results determined with the SMM with those obtained by X-ray diffraction generally calculated using the HM. So, in this study, the SMM is only used to test the L value and all the other tests are made using the HM with a fixed L value.

III. CHARACTERIZATION OF THE PRIMARY RECRYSTALLIZATION TEXTURE OF A Fe 3 pct Si SHEET

The aim of this section is to compare local and global textures measured on three Fe 3 pct Si samples at the surface, at the fifth of the thickness and at the center of a recrystallized sheet. The fifth of the thickness is chosen, because during the final annealing for secondary recrystallization which is performed under hydrogen atmosphere, it was shown that Goss grains grow in the subsurface, *i.e.*, between the fourth and fifth of sheet thickness from the surface. From these comparisons, one can finally evaluate the best values of parameters to assess a good representation of $F(g)$ using the modeling principle of each individual orientation by a Gaussian function.

A. *X-ray Diffraction Study*

The pole figures have been determined by X-ray diffraction in reflection transmission.[26,27] The ODF is determined assuming an orthorhombic symmetry of texture and with $L = 22$. Two main preferential orientations are found:

{111}⟨112⟩: $\bar{F}(g)$ increases from the center of the sheet to the surface ($\bar{F}(g) = 8$ to 10); and
{100}⟨012⟩: $\bar{F}(g)$ decreases from the center to the surface ($\bar{F}(g) = 5$ to 3).

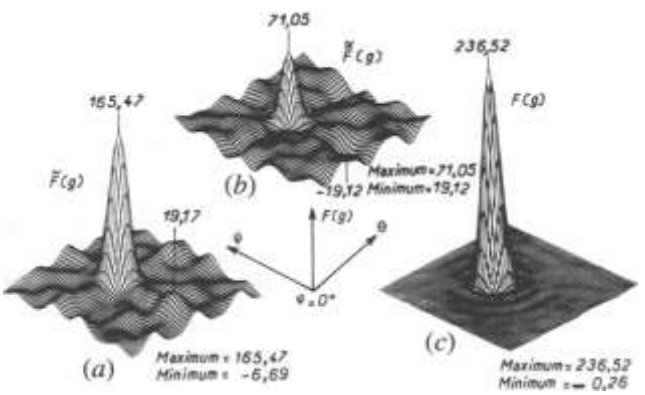

Fig. 2—{011}⟨211⟩ orientation—SMM: (*a*) even part, (*b*) odd part, and (*c*) total texture function.

The sections at $\varphi = 0$ and 45 deg of $\tilde{F}(g)$ are presented in Figure 3 in the case of sample cut off at the center of the sheet. On these section plots, one can see immediately the maximum peaks corresponding to the two preferential orientations:

$\{111\}\langle 112\rangle$ at $\psi = 0$ deg, $\theta = 55$ deg, $\varphi = 45$ deg and $\psi = 60$ deg, $\theta = 55$ deg, $\varphi = 45$ deg; and
$\{100\}\langle 012\rangle$ at $\psi = 20$ deg, $\theta = 0$ deg, $\varphi = 45$ deg and $\psi = 25$ deg, $\theta = 0$ deg, $\varphi = 0$ deg.

Finally, it is important to emphasize that with the X-ray diffraction technique, the Goss component $\{110\}\langle 001\rangle$ was not detected.

Using the MM described earlier, the true ODF $F(g)$ can be evaluated. This calculation is performed with $r_{min} = 0.0$ (the experimental values of $q(\eta,\chi)_{min}$ are near 0.0) and for 20 iterations to obtain a good convergency of maximal and minimal values of $F(g)$. (Note that the number of iterations can be decreased using an optimization parameter[28,29] which was not used in this study since the time factor was not important here.)

Figure 4(a) shows, for the three samples, the evolution of $F(g)_{min}$ as a function of the iteration step (n). A large decrease appears in the absolute values of $F(g)_{min}$ for n less than 10 and then $F(g)_{min}$ remains approximately constant. So this figure shows that convergence is reached after 20 iteration steps. Note (Figure 4(b)) that this convergency is also verified on the $F(g)_{\{111\}\langle 112\rangle}$-$n$ and $F(g)_{\{100\}\langle 012\rangle}$-$n$ curves which show that the evolution of ${}^{(0)}F(g)$ to ${}^{(20)}F(g)$ is about 15 to 20 pct.

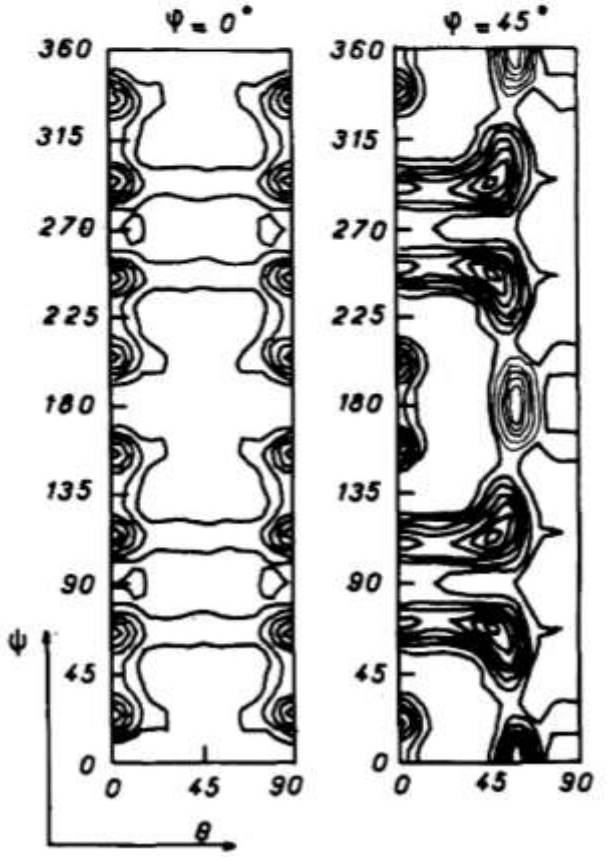

Fig. 3—X-ray diffraction—sample at the center of the sheet thickness $\varphi = 0$ and 45 deg section plots. Intensity levels at 1, 2, . . ., 7.

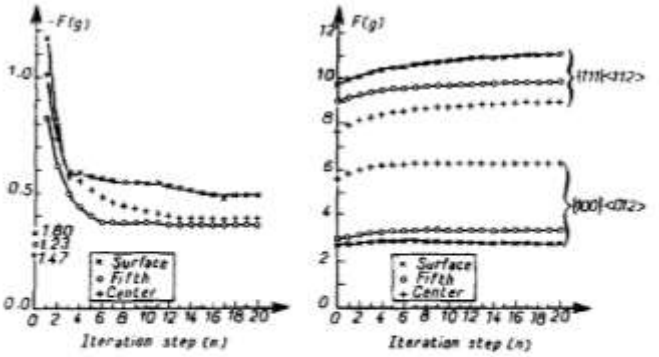

(a) (b)

Fig. 4—Mathematical method: (*a*) evolution of the minimum of $F(g)$ as the iteration step (n); (*b*) evolution of the maxima of $F(g)$ as the iteration step (n).

B. *Single Orientation Measurements*

To measure single orientations from polycrystalline samples, several techniques can be used:

Electron diffraction
- transmission electron microscopy
- selected area channeling patterns
- electron channeling pattern
- electron backscattering pattern

X-ray diffraction
- Kossel pattern
- Laue pattern.

In this study, the EBSP technique, developed by Dingley,[30] is used. The EBSP are KIKUCHI patterns visualized by a phosphorus screen; the pattern is sent to a low level light camera *via* a fiber-optic bundle and then imaged on a TV monitor which is connected to a computer. The patterns are interpreted on line for different classes of crystal symmetry.

For each sample, 1000 individual orientations have been measured with the EBSP technique.[31] Figure 5 shows the {200} pole figures measured on these three samples, by X-ray diffraction and by EBSP techniques.

The $\tilde{F}(g)$ functions are calculated using the HM to $L = 22$ (*i.e.*, in the same conditions as those used for the analysis of data given by X-ray diffraction). Indeed, Rouag[26] has shown that with $L = 22$, the mean square error between experimental and calculated pole densities is less than 5 pct. However, this parameter will be discussed further.

Figures 6(a) through (c) show respectively for the sample cut off at the surface of the sheet, the sections at $\varphi = 45$ deg of $\bar{F}(g)$, $\tilde{F}(g)$, and $F(g)$ in the (ψ,θ) plane. It is interesting to note qualitatively the rather good agreement between $\tilde{F}(g)$ functions calculated using pole figures (Figure 3(b)) and electron diffraction. This result suggests that in a first approximation, the number of orientations is sufficient. However, it seems interesting to optimize this number (see also Reference 19 for an aluminum sheet, Reference 32 for an Fe 3 pct Si sheet, and Reference 33 for a titanium alloy).

From a general point of view, the results obtained using single orientation measurements match those obtained using X-ray diffraction. In particular, the increase of $\bar{F}(g)$

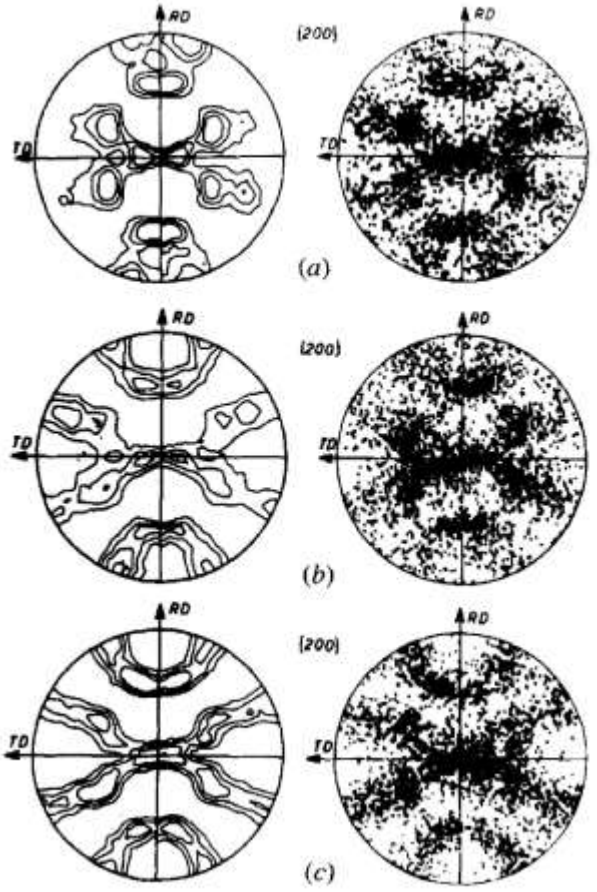

Fig. 5—{200} pole figures. Comparison between X-ray diffraction and electron backscattered diffraction: (*a*) surface, (*b*) fifth, and (*c*) center.

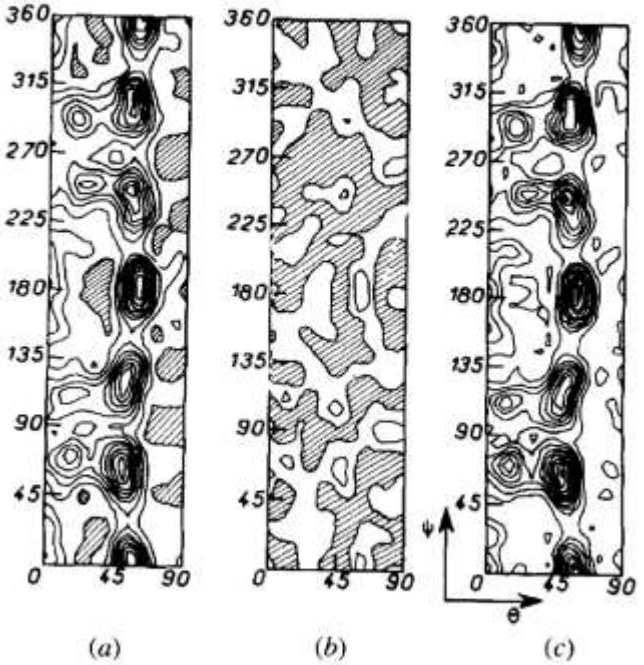

Fig. 6—Sample at the surface of the sheet—$\varphi = 45$ deg section plots of (*a*) $\tilde{F}(g)$, (*b*) $\overline{\tilde{F}(g)}$, and (*c*) $F(g)$. Intensity levels at 0, 1, . . ., 10. ///: negative values.

from the center to the surface of the sheet for the {111}⟨112⟩ orientation and the decrease of $\bar{F}(g)$ for the {100}⟨012⟩ orientation are verified. Moreover, it is interesting to note that the height of $\bar{F}(g)$ is not negligible, since it corresponds to about 15 to 20 pct of $F(g)$ but does not modify the evolution of $F(g)$.

Figures 7(a) through (c) allow comparison of the total texture functions $F(g)$, respectively, for the samples at the surface, at the fifth, and at the center of the sheet. Some negative domains due to truncation errors remain, but they are not drawn because they are negligible. These section plots of $F(g)$ show that the sharpness of $F(g)$ for the {111}⟨112⟩ and {100}⟨012⟩ orientations evolves in the same way as that described before for $\bar{F}(g)$.

So, qualitatively, a rather good agreement is observed. Quantitatively, the results are also similar, particularly when the texture gradient through the sheet thickness is observed (Figure 8). However, a discrepancy is observed for the {100}⟨012⟩ component. This difference, for the sample at the fifth of the sheet thickness, can be due to a shift with respect to the exact position corresponding to the fifth because of the electrolytic polishing.

Using the MM, it is possible to observe the evolution of $F(g)$ through the thickness of the sheet (Figure 8). The discrepancies between these last curves are larger than those observed for $\bar{F}(g)$ and can have the following origins:

(1) the MM tends to minimize the $F(g)$ values (see results presented, for example, by Dahms and Bunge[20]); and
(2) the MM adds errors linked to the determination of $\bar{F}(g)$ using X-ray diffraction and to the calculation method.

It is worth noting that only one Goss grain, among the 3000 studied, was found in the middle of the sheet thickness and not at the fifth. So it is obvious that the volume

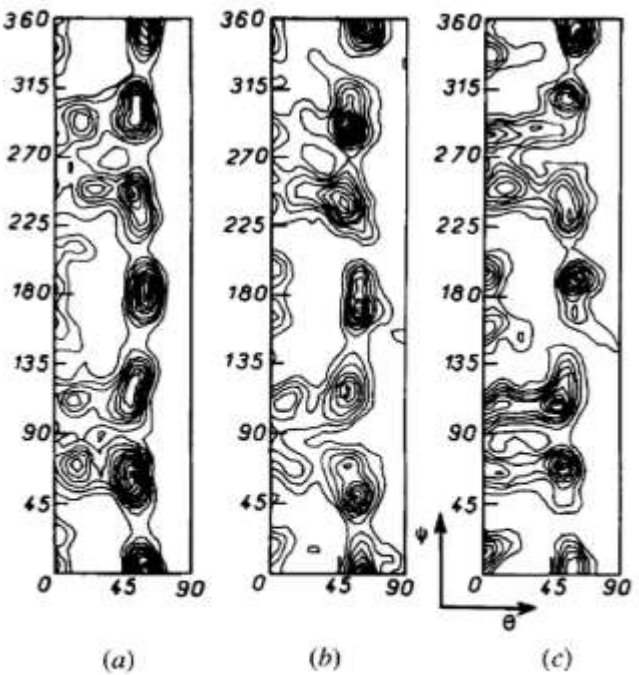

Fig. 7—φ = 45 deg section plots of $F(g)$: (*a*) surface, (*b*) fifth, and (*c*) center. Intensity levels at 1, 2, . . ., 10.

fraction of the Goss grains is very low and that, moreover, they are randomly distributed through the sheet thickness, contrary to the previous assumptions (see also Reference 31).

C. *Discussion*

This study allows the following points to be considered.

(1) The odd part of the ODF is not negligible, since it corresponds to about 15–20 pct of $F(g)$.
(2) The different experimental methods used to calculate $\bar{F}(g)$ give similar results (this remark is also true for $F(g)$) knowing that experimental and numerical errors appear.

So, the above points can explain the observed differences. However, one can verify some of these parameters and, in particular, try to answer the most important question:

"Is the number of individual orientations sufficient to obtain an $F(g)$ function statistically admissible (by comparison with "measurable function," for example, by X-ray diffraction)?"

IV. DISCUSSION OF RESULTS

A. *Influence of the L Parameter*

To verify the results obtained with the EBSP technique, the ODF calculated by Rouag[26] is used. In these conditions, the L value is fixed to 22 (which is sufficient when the measured and calculated pole figures are compared). However, it is interesting to show the influence of L on the $\bar{F}(g)$ (and $F(g)$) evaluation.

For the center of the sheet, Figures 9(a) and (b) show, respectively, the evolution of the $\bar{F}(g)$ and $F(g)$ maxima in terms of the φ Euler angle. These curves are determined using the EBSP technique and calculated with the

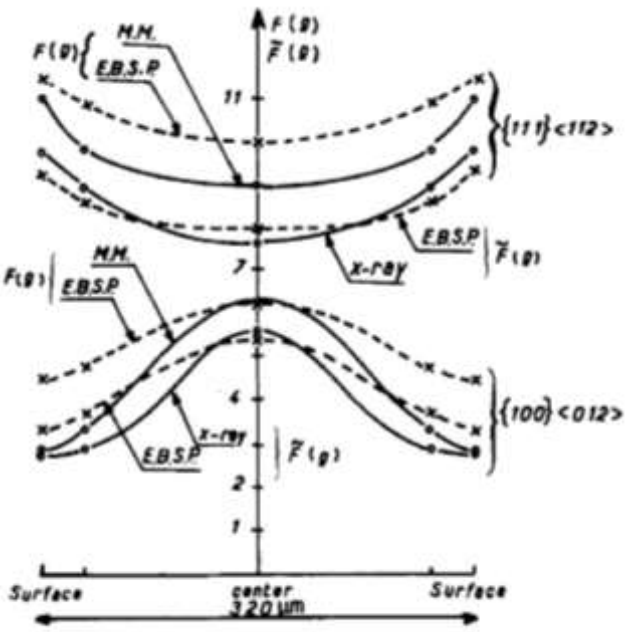

Fig. 8—Texture gradient in the thickness of the sheet.

SMM and the HM with $L = 34$ and 22. They are compared to the $\bar{F}(g)$ values obtained by X-ray diffraction in the first figure and to the $F(g)$ values calculated with the MM in the second case. Note, however, that these last two comparisons allow us to give only an evaluation of error which is perhaps not realistic, since the minimum number of orientations is not tested (the presented results obtained by EBSP technique are determined using 1000 orientations).

If $\bar{F}(g)$ and $F(g)$, determined with the SMM, are the true values, it appears that the HM with $L = 34$ gives a very good solution, particularly for $\bar{F}(g)$. For $F(g)$, the discrepancy between these two curves increases since the $F(g)$ values increase (comparatively to the $\bar{F}(g)$ values), showing that L must be increased. However, the HM with $L = 22$ gives a good approximation of the true result and moreover of the curve determined by X-ray diffraction. This last point is less true for $F(g)$. It is also interesting to remark that the calculation with $L = 22$ leads to some imperfections (see Figure 9(b) at $\varphi = 35$ to 40 deg). It seems that this lack of coincidence of maxima is essentially due to the employment of a grid which can lead to a ψ, θ, and φ shift of 5 deg.

In conclusion, it appears that for our samples (and so for this kind of texture), if the HM is used, the $L = 34$ value must be used to obtain a very good approximation of $\bar{F}(g)$ and $F(g)$. Though the value of $L = 22$ is not

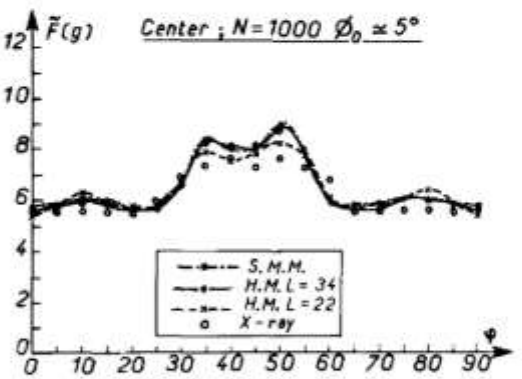

(a)

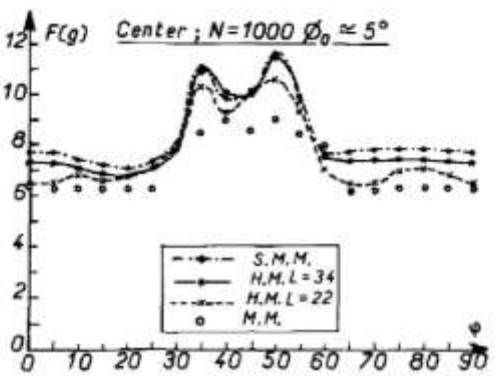

(b)

Fig. 9—Influence of L on the calculation of (a) $\bar{F}(g)$ and (b) $F(g)$.

sufficient, it gives a rather good approximation of $\bar{F}(g)$ and $F(g)$, the aim of this study being the comparison of ODF obtained with the same value of L, so $L = 22$ is kept.

B. *Influence of p Parameter*

To model each individual orientation by a Gaussian function, the Wright and Adams[19] relation (Eq. [10]) is used. This relation allows the Φ_0 parameter to be linked to the number of orientations using the p parameter characterizing the sharpness of the texture. As is the case with some other authors,[13,19] $p = 0.5$, corresponding to an average texture, is chosen arbitrarily. In this section, this parameter is tested to show its influence on the determination of $\bar{F}(g)$ and $F(g)$. Figure 10 allows us to say that for a given L (= 22) value, the p value modifies the texture sharpness but does not modify the shape of $\bar{F}(g) - \varphi$ curves.

To verify the $p = 0.5$ value, the evolutions of $\bar{F}(g)$ and $F(g)$ in terms of p have been observed for the three samples, respectively, in Figures 11(a) through (c). These curves are compared to the maximum values of $\bar{F}(g)$ and $F(g)$ calculated using pole figures and the MM. If the $\{111\}\langle 112\rangle$ orientation is considered, it appears that the intersection of these curves characterizing $\bar{F}(g)$ occurs, respectively, for (a) $p = 0.40$, (b) $p = 0.45$, and (c) $p = 0.60$. So, taking into account the experimental errors, it seems that $p = 0.5$ constitutes a good approximation. For the intersection of the curves characterizing $F(g)$, the p values are larger, so $p = 0.60$, $p = 0.75$, and $p = 0.75$, respectively. However, it has been shown, in our case particularly, that because of experimental errors, the MM minimizes the $F(g)$ values, and if an error of about 10 pct is assumed, the $p = 0.5$ value is found again. Concerning the values of $\bar{F}(g)$ and $F(g)$ for the $\{100\}\langle 012\rangle$ orientation, it is most difficult to conclude, particularly for samples at the surface and at the fifth of the sheet thickness. Indeed, the calculated curves are above the "experimental curves." This problem is essentially linked to reasons, such as experimental errors and number of orientations.

Wright and Adams[19] used a mean square error measurement to describe the difference between two

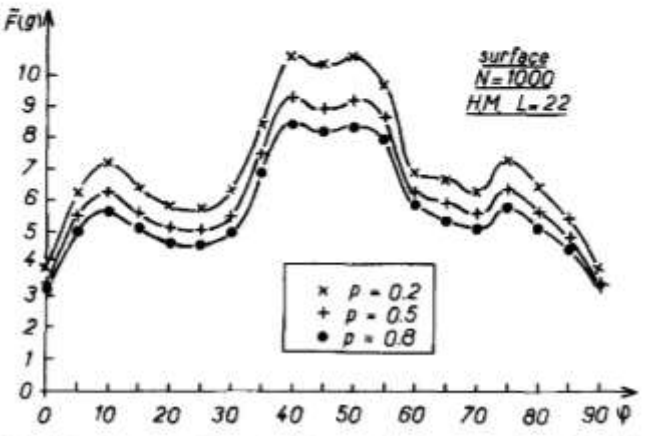

Fig. 10—Influence of p on the $\bar{F}(g)$ calculation for a given L (= 22) value.

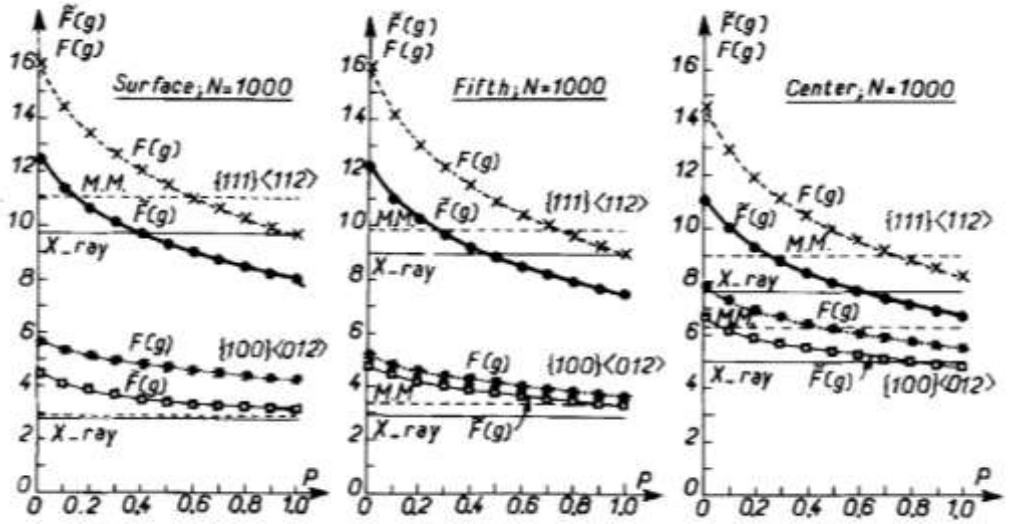

Fig. 11 — Evolution of $\bar{F}(g)$ and $F(g)$ as p: (*a*) surface, (*b*) fifth, and (*c*) center.

ODFs, $F_a(g)$ and $F_b(g)$. This is given by the following equation:

$$\sigma = \sqrt{\frac{1}{J}\sum_{j=1}^{J}[F_a(g_j) - F_b(g_j)]^2} \qquad [20]$$

where the sum was taken over a 5 × 5 × 5 deg grid in Euler space. However, since the texture can be completely characterized by the coefficients of the series expansion, Eq. [20] can be replaced with a modification of the so-called texture index (Bunge[2]), so (see also Roe[3]) with ${}^{ab}f_{lmn} = {}^{a}f_{lmn} - {}^{b}f_{lmn}$,

$$J_{\text{diff}} = \sum_{l,m,n} 4\pi^2 [{}^{ab}f_{lmn}]^2 \qquad [21]$$

This texture difference Index has the advantage over Eq. [20] in that it is not dependent on the "fineness" of the comparison grid in Euler space or the number of comparison points used in the calculation and it also scales with the order of the series expansion. It is easily adaptable for considering both odd and even (J_{diff}), only odd ($\bar{J}_{\text{diff}}$), or only even ($\tilde{J}_{\text{diff}}$) coefficients.

So to complete this analysis of the influence of the p parameter, the square root of the texture difference index (which is homogeneous to the mean square error) is calculated in terms of p.

The evolution of these curves (Figures 12(a) through (c)) shows a large decrease of $(\bar{J}_{\text{diff}})^{1/2}$ and $(J_{\text{diff}})^{1/2}$ for the small values of p (<0.4 to 0.5) and then a small decrease for the large values of p. In this case, it is very difficult to estimate where these curves converge and to determine the p value at this point. However, these curves show that $p = 0.5$ constitutes a good approximation.

The actual results, determined for $N = 1000$, show that when the $L = 22$ and $p = 0.5$ parameters are used, the values of $\bar{F}(g)$ and $F(g)$ are in a good agreement with those determined using pole figure measurements and the MM. Now, the L and p parameters are fixed to analyze the influence of the orientation number.

C. *Influence of N Parameter*

In a first approximation, there appears to be good agreement between results obtained by X-ray diffraction and EBSP, but it is interesting to try to determine the optimum orientation number sufficient to calculate a representative ODF.

Figure 13 shows, for example, for the sample studied at the fifth, the $\varphi = 45$ deg section plots for ODFs calculated using even coefficients for 100, 200, 300, . . ., 1000 orientations, which are compared to the ODFs calculated using pole figures.

It is interesting to note that the principal components of the texture appear only after 100 measurements, and it seems that after 600 measurements, the texture does not change. To determine the optimum orientation number, Wright and Adams[19] proposed calculation of the mean square error (σ) between $F(g)_{100}$, $F(g)_{1000}$, and the classical ODF (respectively, $\sigma = 1.89$ and 0.89). Then, assuming a simple linear evolution, they found that 1800 measurements would be necessary to match the accuracy of the classical ODF. For the three samples studied, the calculation of $(\bar{J}_{diff})^{1/2}$ and $(J_{diff})^{1/2}$ shows that if a simple linear evolution is assumed, the optimum value of N is found between 2000 and 3100 (Figures 14(a) and (b)). However, it appears that this linear evolution assumption constitutes a bad approximation of experimental results.

So, to complete these first results, the maximum values of $\bar{F}(g)$ and $F(g)$ are analyzed in terms of orientation number (Figures 15(a) through (f)). For the three samples and the two orientations, large variations of $\bar{F}(g)$ appear for small values of N, and then $\bar{F}(g)$ tends toward a value which is in a good agreement with the experimental value determined using pole figures. These curves seem to converge when N tends toward about 800 measurements. The evolution of $F(g)$ in terms of N is similar. It is less obvious that the convergence is obtained for the sample at the fifth of the thickness sheet, particularly for the $\{111\}\langle 112\rangle$ orientation. However, it can be seen that the increase of $F(g)$ between 800 and 1000 orientations is lower than between 400 and 600 or 600 and 800. So, it seems that about 800 to 1000 orientations are sufficient to calculate the ODF. To be absolutely sure, it would be necessary to measure more than 1000 orientations on one sample.

To determine the N optimum value, the $\bar{F}(g)$ and $F(g)$-N curves are assumed independent of N when this optimum value is reached. To test this assumption, the measurements on the three samples have been combined to obtained a theoretical sample characterized by 3000 orientations. Note that in the case of neutron diffraction, the pole figures are measured on a bulk sample, so the $F(g)$ maximal value of this sample can be approximated averaging the maximum of the ODF of extreme textures determined by X-ray diffraction. In these conditions, $\bar{F}(g)$ takes the value of 8.7 for the $\{111\}\langle 112\rangle$ orientation and 4.2 for the $\{100\}\langle 012\rangle$ orientation. Obviously, it is a bad approximation, since each set of 1000 orientations has been determined in three particular planes of the sheet and not continuously through the sheet thickness.

Figure 16 shows the evolution of $\bar{F}(g)$ and $F(g)$ maxima for the two principal orientations in terms of the

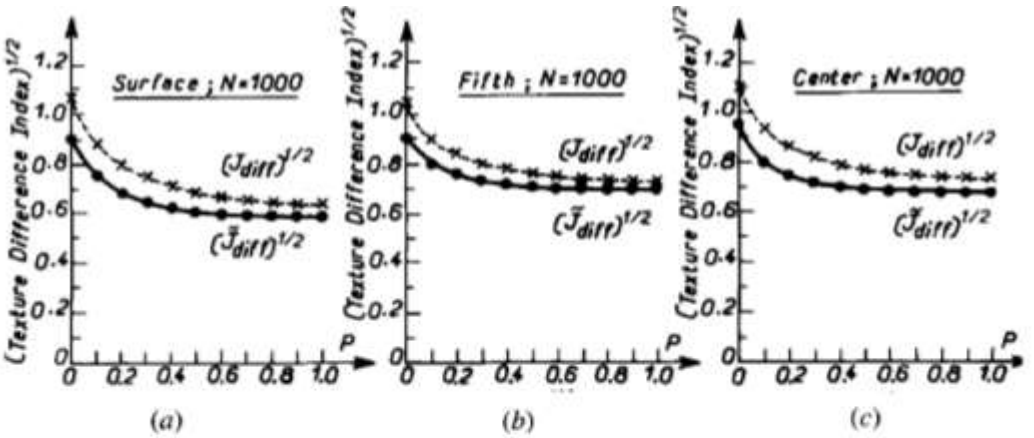

Fig. 12—Evolution of the square root of the texture difference index as p: (*a*) surface, (*b*) fifth, and (*c*) center.

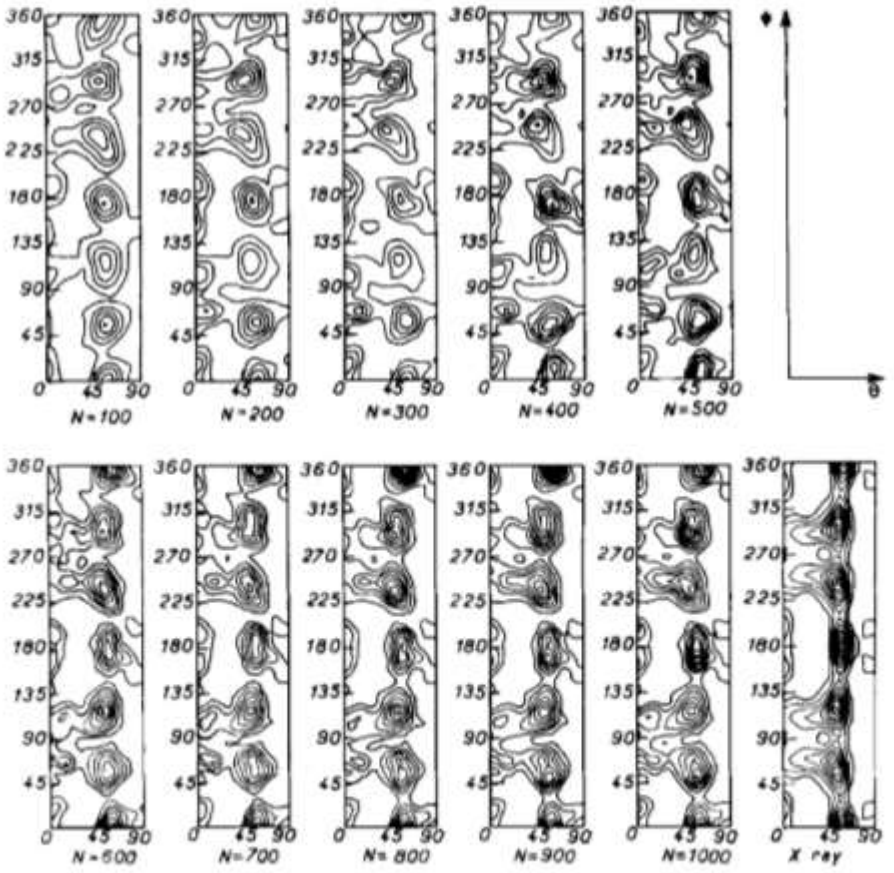

Fig. 13—Sample at the fifth of the sheet thickness—φ = 45 deg section plots of $\bar{F}(g)$ for 100, 200, . . ., 1000 measurements and comparison with X-ray diffraction.

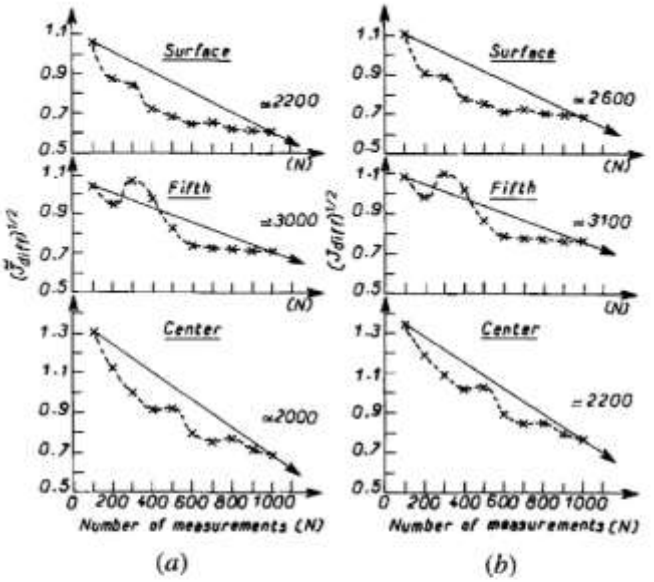

Fig. 14—Evolution of the square root of the texture difference index as N for the three samples: (*a*) $(\bar{J}_{diff})^{1/2}$ and (*b*) $(J_{diff})^{1/2}$.

number of measurements. It appears that the curve corresponding to the first orientation {111}⟨112⟩ is stabilized after about 1500 measurements around a value of 8.3. In the case of the second orientation {100}⟨012⟩, after 100 measures, the $\bar{F}(g)$ value is reached and then fluctuates around a value of 4.2 to 4.3. If, by using these

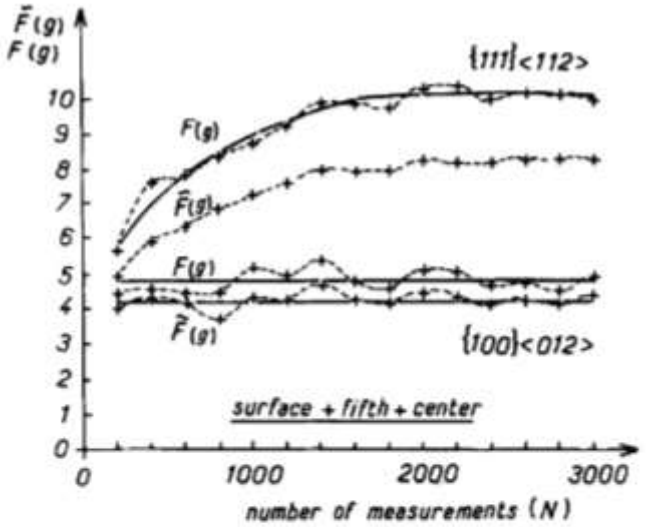

Fig. 16—Evolution of $\bar{F}(g)$ and $F(g)$ as N—3000 measurements.

last curves concerning the second orientation, it is more difficult to evaluate the optimum number of orientations, it is interesting to note that the difference between the minimal and maximal values of $\bar{F}(g)$ on the complete curve (between 200 and 3000 measures) is about 25 pct and only about 8 pct in the domain included between 1500 and 3000 measures. These results show that the stability of the kind of curves shown on Figures 15(a) through (f) is real.

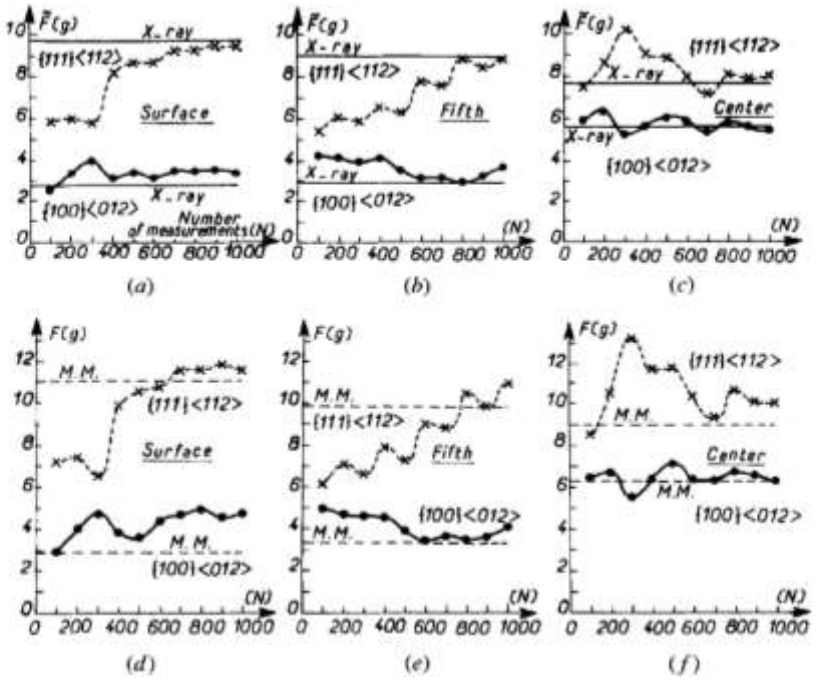

Fig. 15—Evolution of $\bar{F}(g)$ and $F(g)$ as N: (*a*) $\bar{F}(g)$—surface, (*b*) $\bar{F}(g)$—fifth, (*c*) $\bar{F}(g)$—center, (*d*) $F(g)$—surface, (*e*) $F(g)$—fifth, and (*f*) $F(g)$—center.

Thus far only the evolution of $\bar{F}(g)$ and $F(g)$ were studied in terms of the orientation number. To complete this work, the evolution of the pole density ($\bar{q}(\eta,\chi)$) is observed in terms of N. Figure 17 shows the evolution of maximum of {110}, {200}, and {112} calculated pole figures assuming the 3000 orientations. The stability of these curves is absolutely obtained after about 1400 orientations (particularly because of the large variation of $\bar{q}(\eta,\chi)$ of the {200} pole figure for little values of N).

In summary, it appears that to calculate an ODF similar to that determined by X-ray diffraction, about 800 measurements are necessary. On the other hand, to simulate a neutron diffraction measurement, in our case (for a given texture sharpness and a given grain size), it is useful to measure about 1500 orientations. Obviously, this last N estimate is linked to the texture gradient, so Figure 18 shows that for 2000 combined orientations using orientations measured at the fifth and at the center of the sheet (because the texture gradient between these two samples is weak), the evolution of $\bar{F}(g)$ and $F(g)$ in terms of N begins to stabilize after about 1000 measurements (between 800 and 1500). Indeed, after 1000 orientation measurements, the values of $\bar{F}(g)$ and $F(g)$ do not vary in large proportions: for the {111}⟨112⟩ orientation, the variations around an average value are about 5 pct, and for the {100}⟨012⟩, about 7 pct.

D. *Influence of Sample Symmetry*

Rouag[26] has calculated the ODF using pole figures with an orthotropic texture symmetry, whereas all calculations using individual orientations are performed with a triclinic texture symmetry. It is interesting to verify the discrepancy with respect to the orthotropic symmetry. Figure 19 shows, for example, the case of the 3000 measurements. Since in the case of triclinic symmetry, the ψ domain includes four domains of ψ corresponding to the orthotropic symmetry, four maximum values of $\bar{F}(g)$ and $F(g)$ can be determined for each {111}⟨112⟩ and {100}⟨012⟩ orientation. These curves show that the difference with respect to the orthotropic symmetry is not very important, and so the calculation can be made with

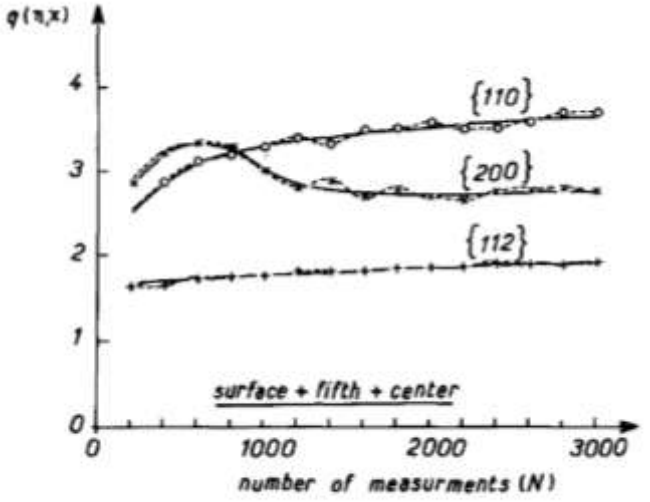

Fig. 17—Evolution of $q(\eta,\chi)$ as N for {110}, {200}, and {112} pole figures—3000 measurements.

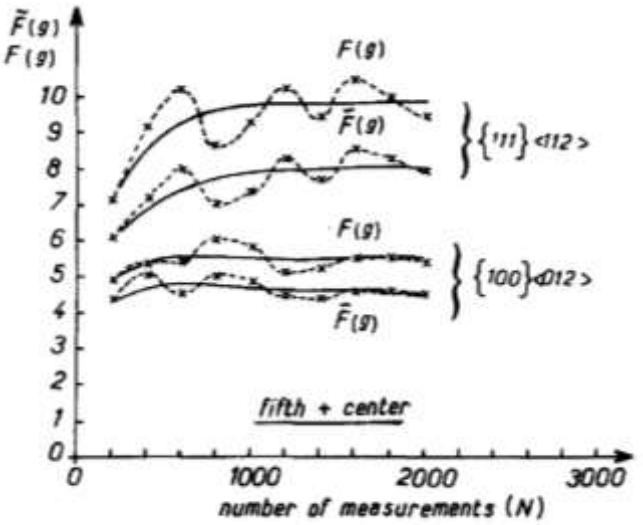

Fig. 18—Evolution of $\bar{F}(g)$ and $F(g)$ as N—2000 measurements.

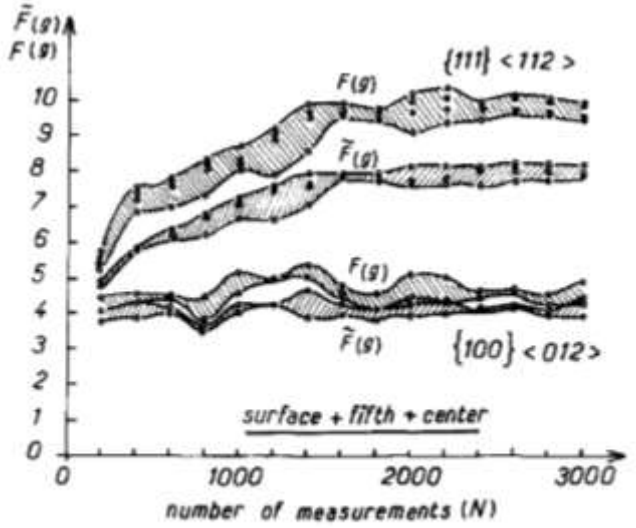

Fig. 19—Evolution of $\bar{F}(g)$ and $F(g)$ as N—3000 measurements. Evolution of the discrepancy to the orthotropic symmetry of texture.

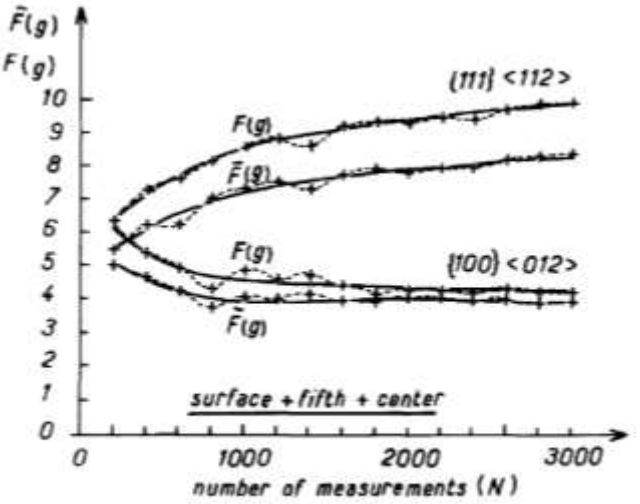

Fig. 20—Evolution of $\bar{F}(g)$ and $F(g)$ as N—3000 measurements; orthotropic symmetry of texture.

the orthotropic symmetry. In these conditions, Figure 20 shows the evolution of $\bar{F}(g)$ and $F(g)$ in terms of N for the two main orientations. The point where the stability of these curves occurs is not easy to determine, since for the {111}⟨112⟩ orientation, $\bar{F}(g)$ and $F(g)$ increase continuously to N equal 3000 measurements. However, one can see that after some relatively large variations to about 1600 measurements, these variations vanish and at this point the $\bar{F}(g)$ and $F(g)$ values are not very different than the values at 3000 measurements (error lower than 10 pct). Consequently, this example shows that the influence of the sample symmetry is not very important for the ODF calculation.

E. *Discussion*

To determine a total ODF using the EBSP technique, it is necessary to test some parameters which appear in this kind of calculation. The most important is the number of measurements. This parameter is related to other ones, such as the texture sharpness and the grain size. So, for example, if a scanning domain of 80 mm^2 is assumed, if the grain diameter is about 0.5 mm, 400 grains are measured in X-ray diffraction, and if this diameter is equal to about 50 μm, 40,000 grains are taken into account if the grains are modeled by spheres. In the case of studied samples, it appears that these 40,000 orientations can be replaced by about 1000 to obtain a statistically admissible texture function.

Finally, note that this orientation number allows us to calculate the texture function to a rather good approximation, particularly for the sample at the center, because the sharpness of the two principal orientations is not very different. For the two other samples, the agreement remains satisfactory; however, the discrepancy between ODF values calculated from pole figures and from individual orientations increases for the {100}⟨012⟩ orientation. This phenomenon can be due to some experimental or numerical errors but can also be explained by an orientation number which is perhaps not sufficient when the secondary orientation is close to the "background." In this last case, to verify the orientation number, it is necessary to measure more than 1000 orientations on each sample.

V. CONCLUSION

It seems that 1000 individual orientations allow us to estimate with good agreement a texture function determined using pole figures. Moreover, this technique is very interesting comparatively to the global techniques, such as X-ray and neutron diffraction, since it allows us to calculate directly a total ODF and also to link the orientations of grains to their positions in the sample. So, with the new developments in automatic orientations measurements,[34] (see, for example, Wright *et al.*,[35] who can measure 1800 orientations per hour), they can replace advantageously the global techniques. However, this technique cannot be used in the case of heavily cold-worked materials. Indeed, when the coherent domains of diffraction are smaller than the beam size, the Kikuchi patterns are difficult to interpret.

The aim of this work was principally the evaluation of the orientation number to assess the texture function of a Fe 3 pct Si sheet. The results are so determined for a given material and for a given texture and cannot be directly extrapolated to other materials (or to the same material with different texture) or to solve other problems, such as, for example, the determination of speciality of grain boundaries.[32]

ACKNOWLEDGMENTS

The authors would like to thank Professors B.L. Adams and H. Hu and Doctor J. Jura for very fruitful discussions and a critical reading of the manuscript.

REFERENCES

1. H.J. Bunge: Z. *Metallkd.*, 1965, vol. 56, pp. 827-74.
2. H.J. Bunge: *Texture Analysis in Materials Science*, Butterworth's, London, 1982.
3. R.J. Roe: *J. Appl. Phys.*, 1965, vol. 36, pp. 2024-31.
4. R.J. Roe: *J. Appl. Phys.*, 1966, vol. 37, pp. 2069-72.
5. R.O. Williams: *J. Appl. Phys.*, 1968, vol. 39, pp. 4329-35.
6. D. Ruer and R. Baro: *Adv. X-ray Anal.*, 1977, vol. 20, pp. 187-200.
7. A. Vadon: Ph.D. Thesis, University of Metz, France, 1981.
8. H. Schaeben, A. Vadon, and H.R. Wenk: In *Preferred Orientation in Deformed Metals and Rocks: an Introduction to Modern Texture Analysis*, Academic Press, Orlando, FL, 1985, pp. 123-37.
9. J. Imhof: *Phys. Status Solidi B*, 1983, vol. 110, pp. 693-701.
10. J. Imhof: *Phys. Status Solidi B*, 1983, vol. 110, pp. 321-28.
11. J. Pospiech: *Proc. ICOTOM 8*, Santa Fé, NM, Sept. 1987, J.S. Kallend and G. Gottstein, eds. TMS Warrendale, PA, 1988, pp. 93-104.
12. S. Matthies, G.W. Vinel, and K. Helming: *Standard Distribution in Texture Analysis*, Akademie-Verlag, Berlin, 1987.
13. F. Wagner: Ph.D. Thesis, University of Metz, France, 1983.
14. W. Truszkowski, J. Pospiech, J. Jura, and B. Major: *Proc. 3ème Colloque Européen sur les Textures de Déformation et de Recristallisation des Métaux et Leurs Applications Industrielles*, Pont-à-Mousson, France, R. Penelle, ed., Société Française de Métallurgie, 1973, pp. 235-57.
15. H.J. Virnich, J. Pospiech, A. Flemmer, and K. Lücke: *Proc. ICOTOM 5*, Aachen, Mar. 1978, G. Gottstein and K. Lücke, eds., Springer-Verlag, Berlin, 1978, pp. 129-38.
16. J. Pospiech, K. Lücke, and J. Jura: *Proc. ICOTOM 6*, Tokyo, Sept.–Oct. 1981, The Iron and Steel Institute of Japan, Tokyo, 1981, pp. 1390-1401.
17. K. Lücke, J. Pospiech, K.H. Virnich, and J. Jura: *Acta Metall.*, 1981, vol. 29, pp. 167-85.
18. F. Wagner, H.R. Wenk, C. Esling, and H.J. Bunge: *Phys. Status Solidi A*, 1981, vol. 67, pp. 269-85.
19. S.I. Wright and B.L. Adams: *Textures and Microstructures*, 1990, vol. 12, pp. 65-76.
20. M. Dahms and H.J. Bunge: *Textures and Microstructures*, 1988, vol. 10, pp. 21-35.
21. C. Esling: Ph.D. Thesis, University of Metz, France, 1981.
22. P. Van Houtte: *Textures and Microstructures*, 1983, vol. 6, pp. 1-20.
23. F. Wang, J. Xu, and Z. Liang: *Textures and Microstructures*, 1989, vol. 10, pp. 217-26.
24. H.J. Bunge: *Proc. ICOTOM 8*, Santa Fé, NM, Sept. 1987, J.S. Kallend and G. Gottstein, eds., TMS, Warrendale, PA, 1988, pp. 69-78.
25. F. Wagner, M. Humbert, C. Esling, and J. Muler: *Proc. ICOTOM 9*, Avignon, Sept. 1990, appeared in *Textures and Microstructures*, 1992, vol. 14–18, pp. 45-51.
26. N. Rouag: Ph.D. Thesis, University of Orsay, 1988.
27. N. Rouag and R. Penelle: *Textures and Microstructures*, 1989, vol. 11, pp. 203-17.
28. F. Wagner, M. Humbert, J. Muller, and C. Esling: *Europhys. Lett.*, 1990, vol. 11 (5), pp. 479-83.
29. F. Wagner and M. Dahms: *Advances and Applications of Quantitative Texture Analysis*, H.J. Bunge and C. Esling, eds., DGM Oberursel, 1991, pp. 101-08.
30. D.J. Dingley: *Proc. ICOTOM 8*, Santa-Fé, Sept. 1987, J.S. Kallend and G. Gottstein, eds., TMS, Warrendale, PA, 1988, pp. 189-94.
31. R. Penelle, T. Baudin, P. Paillard, and L. Mora: *Proc. ICOTOM 9*, Avignon, Sept. 1990, C. Esling, R. Penelle, H. Bunge, eds., appeared in *Textures and Microstructures*, 1992, vol. 14–18, pp. 597-610.

32. T. Baudin, P. Paillard, and R. Penelle: *J. Appl. Cryst.*, 1992, vol. 25, pp. 400-08.
33. R. Penelle and T. Baudin: *Proc. Microscale Textures of Materials*, Cincinnati, OH, Oct. 1991, appeared in *Textures and Microstructures*, 1993, vol. 20, pp. 165-77.
34. B.L. Adams: Brigham Young University, Provo, UT, private communication, 1992.
35. S.I. Wright, B.L. Adams, and K. Kunze: Los Alamos National Laboratory, Los Alamos, NM, and Brigham Young University, Provo, UT, unpublished research, 1992.